Rab18 is not necessary for lipid droplet biogenesis or turnover in human mammary carcinoma cells

Christina B. K. Jayson[a,b,†], Henning Arlt[a,b,†], Alexander W. Fischer[a,b,c], Zon Weng Lai[a,b], Robert V. Farese, Jr.[a,b,d,§,*], and Tobias C. Walther[a,b,d,e,§,*]

[a]Department of Genetics and Complex Diseases, Harvard T. H. Chan School of Public Health, and [b]Department of Cell Biology, Harvard Medical School, Boston, MA 02115; [c]Department of Biochemistry and Molecular Cell Biology, University Medical Center Hamburg-Eppendorf, DE-20246 Hamburg, Germany; [d]Broad Institute of MIT and Harvard, Cambridge, MA 02142; [e]Howard Hughes Medical Institute, Boston, MA 02115

ABSTRACT **Rab GTPases recruit peripheral membrane proteins and can define organelle identity. Rab18 localizes to the endoplasmic reticulum (ER) but also to lipid droplets (LDs), where it has been implicated in effector protein recruitment and in defining LD identity. Here, we studied Rab18 localization and function in a human mammary carcinoma cell line. Rab18 localized to the ER and to LD membranes on LD induction, with the latter depending on the Rab18 activation state. In cells lacking Rab18, LDs were modestly reduced in size and numbers, but we found little evidence for Rab18 function in LD formation, LD turnover on cell starvation, or the targeting of several proteins to LDs. We conclude that Rab18 is not a general, necessary component of the protein machinery involved in LD biogenesis or turnover.**

Monitoring Editor
Francis A. Barr
University of Oxford

Received: May 8, 2018
Revised: Jun 12, 2018
Accepted: Jun 19, 2018

INTRODUCTION

How organelles achieve their specific identity is a central question for cell biology. Key for determining the identity of many membrane-bound organelles are small GTPases of the Rab family (Soldati *et al.*, 1995; Stenmark, 2009; Hutagalung and Novick, 2011). These proteins are switchlike molecules that regulate recruitment of specific proteins to membranes. In the inactive, guanosine diphosphate (GDP)-bound state, Rab proteins bind to GDP-dissociation inhibitor (GDI) chaperones in the cytosol. Membrane-bound guanine nucleotide exchange factors (GEFs) on specific organelles activate Rabs by removing the bound nucleotide, allowing the binding of GTP and switching the protein to an active conformation (Pfeffer, 2001; Barr, 2013). Once activated, they provide binding surfaces to recruit effector proteins with functions specific to the organelle. Through such a mechanism, each organelle of the endomembrane system contains specific Rab proteins that act to determine its identity (Barr, 2013).

Lipid droplets (LDs) are cellular organelles found in most cells that store neutral lipids, such as triacylglycerols (TG) and sterol esters, as precursors for cellular membrane lipids and as reservoirs for metabolic energy (Walther and Farese, 2012; Gross and Silver, 2014; Pol *et al.*, 2014). Among cellular organelles, LDs are unique because they are bounded by a monolayer of phospholipids rather than a bilayer membrane (Tauchi-Sato *et al.*, 2002). Liquid dropletss bind specific proteins, and the principles of protein targeting to LDs are just beginning to be understood (Wilfling *et al.*, 2013; Kory *et al.*, 2016; Rowe *et al.*, 2016; Čopič *et al.*, 2018; Prévost *et al.*, 2018). How the identity of LDs is determined molecularly is poorly understood: neither specific lipid species nor Rab proteins that define droplet identity have been identified.

Among Rab proteins, evidence suggests Rab18 may be important for LD identity. Rab18 localizes to the endoplasmic reticulum (ER) (Gerondopoulos *et al.*, 2014) and to LDs (Martin *et al.*, 2005; Ozeki *et al.*, 2005) in several different human and mouse cell lines. Depletion of Rab18 causes defects in ER tubule integrity and affects LD morphology and protein localization to LDs (Martin *et al.*, 2005; Ozeki *et al.*, 2005; Carpanini *et al.*, 2014; Gerondopoulos *et al.*, 2014). The overexpression of Rab18 increases apposition of ER and LD membranes, possibly indicating a role for the protein at ER–LD contact sites (Ozeki *et al.*, 2005). Consistent with these findings,

This article was published online ahead of print in MBoC in Press (http://www.molbiolcell.org/cgi/doi/10.1091/mbc.E18-05-0282) on June 27, 2018.

†These authors contributed equally.

§These authors contributed equally.

*Address correspondence to: Tobias C. Walther (twalther@hsph.harvard.edu) and Robert V. Farese, Jr. (robert@hsph.harvard.edu).

Abbreviations used: ER, endoplasmic reticulum; KO, knockout; LD, lipid droplet; TG, triacylglycerol; WT, wild type.

Rab18 has been implicated in LD biogenesis at the ER by recruiting the NAG-RINT1-ZW10 (NRZ) tethering complex and SNARE proteins (Gillingham *et al.*, 2014; Xu *et al.*, 2018). These findings suggest that Rab18 is a determinant of LD organelle identity. However, this hypothesis has not been extensively tested, and the function of Rab18 at LDs is unclear.

Here we tested whether Rab18 has a direct role in LD homeostasis by studying the protein in mammalian cells. Although we found that Rab18 localizes to LDs, we surprisingly found no evidence of a direct role for Rab18 in LD homeostasis with respect to LD formation, the targeting of selected LD proteins, or TG turnover. This suggests that Rab18 is not required for the basic machinery of these processes.

RESULTS AND DISCUSSION

Rab18 localizes to LDs and the ER

To investigate the role of Rab18 in LD biology, we first analyzed its subcellular localization. We chose to study Rab18 in SUM159 cells (Flanagan *et al.*, 1999), a human mammary carcinoma cell line that we use extensively to study LD biology. These cells 1) express both TG synthesis enzymes, DGAT1 and DGAT2, 2) generate LDs readily on incubation with fatty acid-containing medium, 3) express factors involved in LD biogenesis (including seipin, FIT2, and perilipins 3 and 4; (Bulankina *et al.*, 2009; Gross *et al.,* 2011; Wilfling *et al.,* 2014a; Choudhary *et al.*, 2015; Wang *et al.*, 2016)), and 4) are diploid and amenable to clustered regularly interspaced short palindromic repeats (CRISPR)-based genome engineering and microscopy imaging (Wang *et al.,* 2016; Gluchowski *et al.*, 2017). Additionally, SUM159 cells express Rab18 (see below).

We expressed green fluorescent protein (GFP)-Rab18 in these cells, and imaging by spinning-disk confocal microscopy showed that Rab18 colocalized with the calreticulon-KDEL ER marker mCherry-ER3 (Figure 1A). When cells were treated with oleate for 18 h to induce LD formation, we found that Rab18 localized to LDs (stained with LipidTox) (Figure 1A), as reported (Martin *et al.*, 2005; Ozeki *et al.*, 2005; Li *et al.,* 2016).

We determined whether the localization of Rab18 to LDs depends on the activation state of Rab18. We found that the hydrolysis-deficient mutant Rab18Q67L, which is locked in the active, GTP-bound form, localized to LDs with fatty acid loading, whereas the nucleotide-binding deficient, inactive Rab18S22N mutant was absent from LDs and instead localized to discrete puncta on the ER (Figure 1A).

Overexpression of Rab18 induces close apposition of ER and LD membranes (Ozeki *et al.*, 2005), which might confound localization interpretations. To distinguish between direct localization of Rab18 to LDs versus ER localization close to LDs, we used structured illumination microscopy (SIM), which provides greater imaging resolution than confocal microscopy. We analyzed colocalization of GFP-Rab18 with the luminal ER marker mCherry-ER3. We found that Rab18 localizes to both ER and LDs, with a portion of the signal clearly localizing to LDs and distinct from the ER marker (Figure 1, B and C).

To complement the microscopy studies, we also determined the localization of endogenous Rab18 by examining its biochemical fractionation behavior. In oleate-loaded cells, we detected Rab18 in total lysate and LD fractions, which were enriched for the LD marker proteins PLIN3 and PLIN4 (Figure 1D). Other ER proteins, such as reticulon and calnexin, were absent from the LD fraction, but readily detected in the total lysate (Figure 1D). Our results indicate that Rab18 is an ER-localized protein in SUM159 cells that becomes activated and localizes in part around LDs on their formation.

Deletion of Rab18 does not affect the structure of the ER

Rab18 has been implicated in LD and ER function by overexpression and depletion experiments, but it is unclear whether Rab18 is required for LD biogenesis or turnover. This may be due to the difficulties in interpreting overexpression experiments or residual Rab18 activity in cells with RNAi-mediated depletion of the protein (Martin *et al.*, 2005; Ozeki *et al.*, 2005; Gerondopoulos *et al.,* 2014). To overcome the latter problem, we generated a knockout cell line by CRISPR/Cas9-mediated genome editing. Using this technology, we isolated a SUM159 cell clone with two alleles of Rab18 that were mutated to generate a premature stop codon at the beginning of exon 5, which results in depletion of Rab18 mRNA levels and a complete absence of the protein by Western blot and mass spectrometry analyses (Figure 2, A–D). To rule out clone-specific effects, we also generated a second clone with a 172-bp deletion in exon 5 of both alleles, which results in a premature stop codon. We then evaluated both knockout clones in each of the following experiments.

Since Rab18 is an ER-localized protein in standard culture conditions, we first investigated ER morphology in wild-type (WT) and Rab18 knockout cells. Compared with control cells, Rab18 knockout cells appeared to have normal ER when analyzed by immunofluorescence with antibodies directed against the tubular ER protein Rtn4 or by in vivo fluorescence microscopy using GFP-ERox (Figure 2E). Reintroduction of GFP-Rab18 into Rab18 knockout cells revealed no differences in its localization compared with that found in wild-type cells (Supplemental Figure S1).

Rab18 is not required for LD biogenesis, but Rab18 deletion modestly reduces the size and numbers of LDs

The dual localization of Rab18 to ER and LD membranes on LD induction prompted us to test whether Rab18 is involved in LD biogenesis. We monitored LD size and number on induction of LD biogenesis by addition of oleate to the culture medium of control and Rab18 knockout SUM159 cells. Whereas LDs appeared similar in both cell types at 2 h after oleate addition, there was a modest reduction in the numbers and areas of LDs in Rab18 knockout clones after 24 h (Figure 3, A–C). By using radioactive oleate as a tracer, we found no differences in TG accumulation between Rab18 knockout and wild-type cells (Figure 3, D and E), suggesting that any changes in LD accumulation were not due to changes in TG synthesis rates.

Deletion of Rab18 does not affect the targeting of several key proteins to LDs

During LD biogenesis, several enzymes of the TG synthesis pathway localize to LDs, including ACSL3, GPAT4, and DGAT2 (Stone *et al.,* 2009; Kassan *et al.*, 2013; Wilfling *et al.*, 2013). These proteins, known as class I proteins, are anchored to the membrane by hydrophobic sequences that are embedded in the bilayer membrane and the LD surface. Thus, moving them from the ER to LDs for targeting to LDs requires a membrane continuity or membrane bridge (Wilfling *et al.*, 2013; Wilfling *et al.,* 2014b). Since Rab proteins regulate membrane tethering and fusion reactions, as well as membrane contacts (Hutagalung and Novick, 2011; Hönscher *et al.*, 2014), we hypothesized that Rab18 may be involved in establishing ER–LD bridges for class I membrane protein targeting to LDs. We first tested targeting of GPAT4-GFP to LDs after treatment of cells with oleate for 24 h. As found in control cells, deletion of Rab18 did not affect the dual localization of GPAT4 to ER and LD membranes (Figure 4A).

To further test localization of proteins involved in key aspects of LD biology, we examined adipose triglyceride lipase (ATGL), a TG hydrolase that localizes to LDs via membrane-embedded targeting sequences (Schweiger *et al.*, 2008; Soni *et al.*, 2009). Like GPAT4,

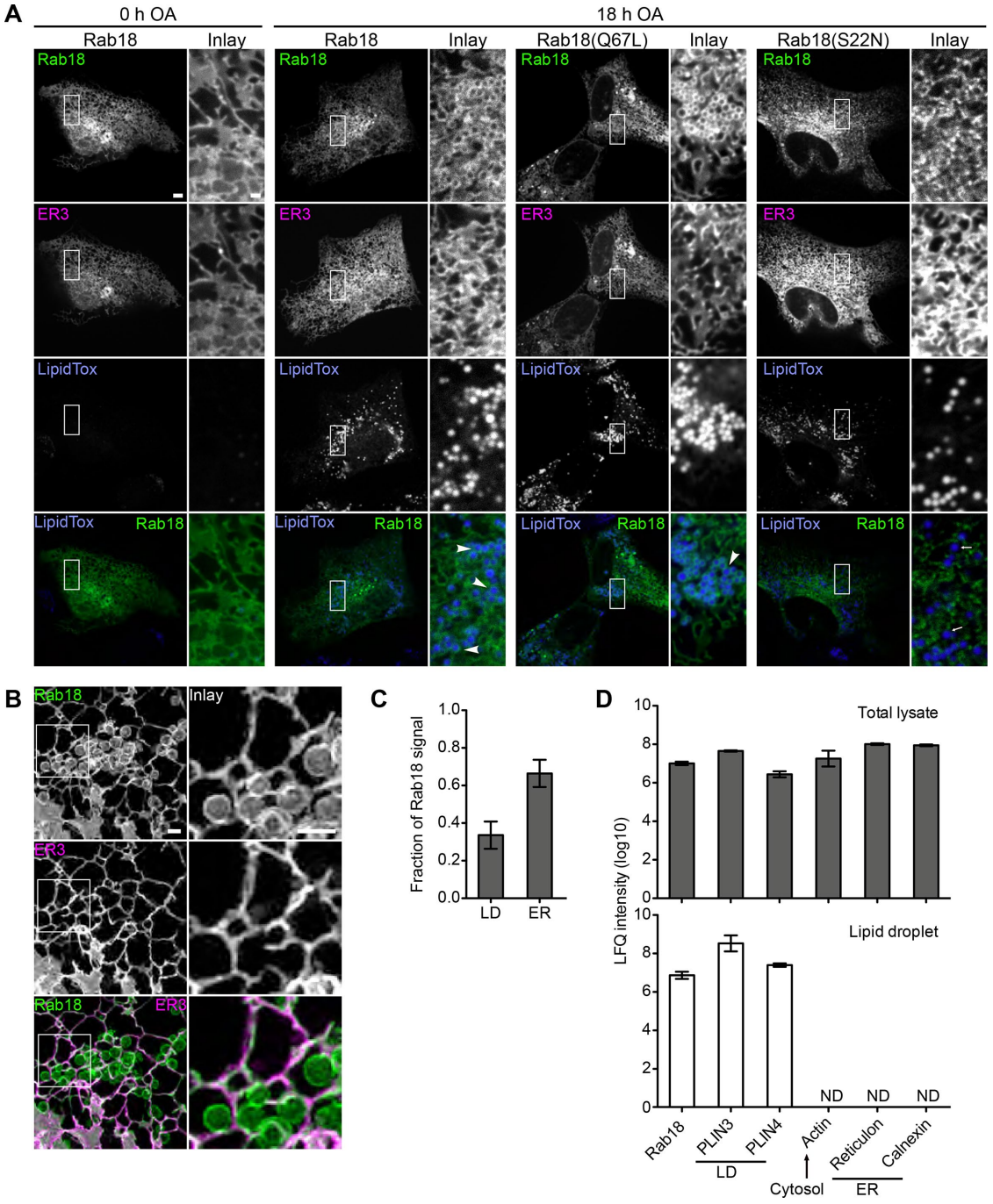

FIGURE 1: Rab18 localizes distinctly to LDs and the ER in SUM159 cells. (A) Overexpressed GFP-Rab18 localizes to LDs (LipidTox) (white arrowheads) and the ER (mCherry-ER3), and localization depends on GTP state (white arrows). SUM159 cells coexpressing mCherry-ER3 and GFP-tagged WT Rab18, GDP-bound Rab18(S22N) mutant, or GTP-bound Rab18(Q67L) mutant were incubated with OA for 0 or 18 h and imaged with spinning disk confocal. Scale bar 5 μm and for inlay 1 μm. (B) Rab18 localizes to the ER and LD structures. SUM159 cells co-expressing mCherry-ER3 and GFP-Rab18 were incubated with oleic acid for 18 h and imaged by SIM. Max projections of 1.25-μm stacks are shown. Scale bars, 1 μm. (C) Quantification of Rab18 signal distribution in SIM images. $n = 5$ fields. (D) Rab18 was detected in LD fractions and total cell lysates of SUM159 cells. LD fractions and cell lysates isolated from SUM159 cells after 18 h oleic acid were analyzed by mass spectrometry to detect proteins on LDs compared with total lysate. ND = not detected.

ATGL localization depends on Arf1/COPI proteins (Soni *et al.*, 2009) and may occur via ER–LD bridges. We expressed a fluorescently tagged catalytically inactive mutant of ATGL that localizes to LDs (Smirnova *et al.*, 2006). Similarly to the findings for GPAT4, targeting of ATGL to LDs was unaffected by the absence of Rab18 (Figure 4B).

Class II proteins localize to the LD monolayer directly from the cytosol by inserting one or several amphipathic helices into the monolayer of the LD surface (Bussell, 2005; Prévost *et al.*, 2018). We examined the localization of PLIN3, a class II protein, and also did not detect differences in targeting for Rab18 knockout and

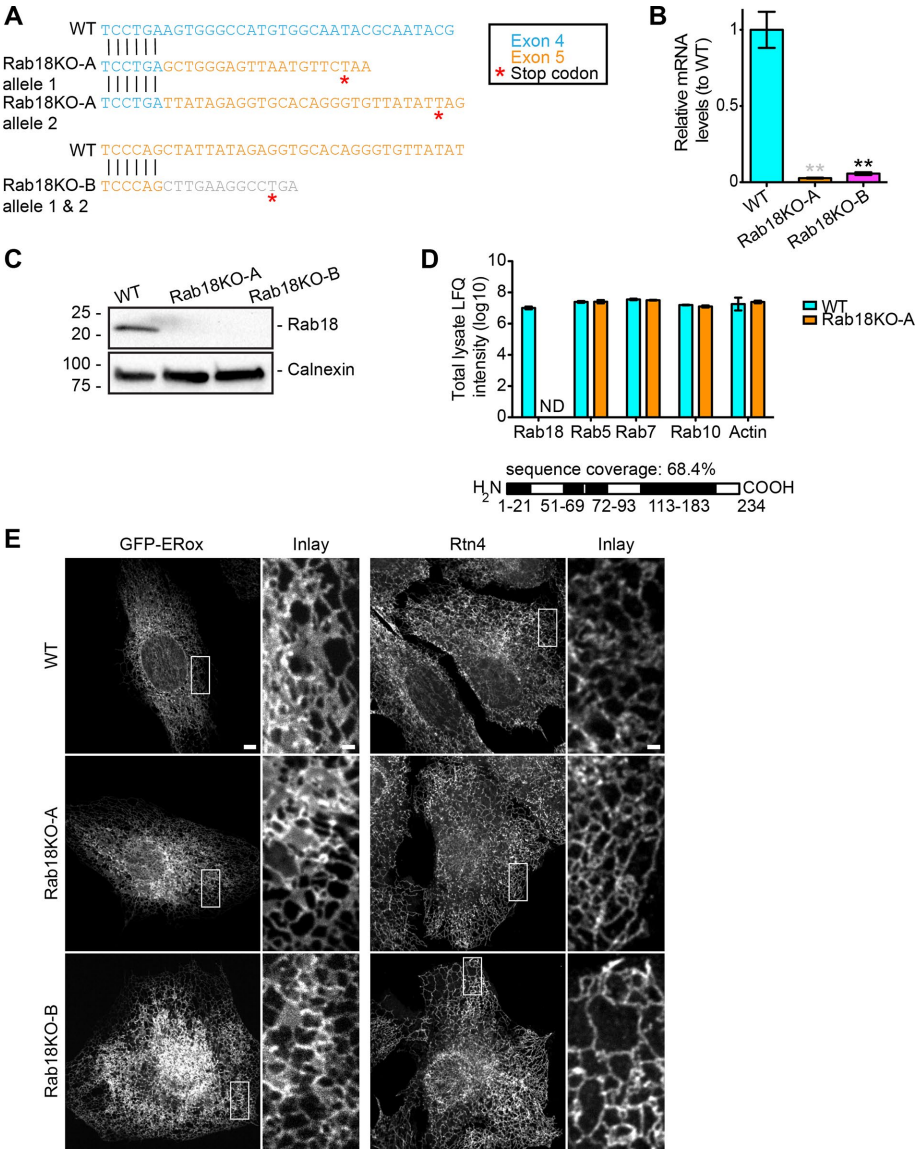

FIGURE 2: Rab18 deletion does not affect ER morphology. (A) Sequence analysis of Rab18 KO clones A and B. CRISPR/Cas9-mediated genome editing of the Rab18 locus introduces early stop codons at exons 4 (clone A) and 5 (clone B). (B) qPCR data reveal decreased Rab18 mRNA levels by 98 and 96% in Rab18KO-A and –B, respectively, compared with WT control. WT vs. Rab18KO-A* in gray, WT vs. Rab18KO-B* in black. (C) No Rab18 protein is detected in knockout clones by Western blot. Expression levels of Rab18 protein in WT and Rab18 KO cells were analyzed by Western blot with an antibody against endogenous Rab18. No detectable Rab18 protein was found in the Rab18KO-A or Rab18KO-B. (D) Rab18 peptide fragments were not detected by mass spectrometry in Rab18KO-A. WT SUM159 cell lysates and Rab18KO-A cell lysates were analyzed by mass spectrometry with sequence coverage of 68.4% for Rab18. (E) ER morphology in Rab18 KO clones is similar to WT cells. Cells were transfected with GFP-ERox to analyze general ER morphology. Separately, cells were fixed and probed with Reticulon 4 (Rtn4) antibody to visualize ER tubules. Scale bar 5 µm and for inlay 1 µm.

wild-type cells (Figure 4C). Thus, Rab18 is not required for targeting of two ER proteins (GPAT4 and ATGL) or one cytosolic protein (PLIN3) that localize to LDs.

Deletion of Rab18 has no effect on triglyceride turnover during cell starvation

Induction of lipolysis in cultured adipocytes increases Rab18 targeting to LDs (Martin *et al.*, 2005; Pulido *et al.*, 2011). We thus tested the hypothesis that Rab18 may be involved in turnover of LD-stored TGs. We generated cells with abundant LDs (incubating them in oleate containing medium for 12 h) and induced starvation and TG turnover by removing fetal bovine serum (FBS), insulin, and oleate from the culture medium. We found that, by 48 h of starvation, most LDs were degraded (Figure 5A). When we analyzed LD size and numbers (by boron-dipyrromethene [BODIPY] staining using high-throughput microscopy and automated image analysis) during a time course of LD catabolism, Rab18 knockout cells (and in particular one clone) showed evidence of increased turnover of LDs, but after 48 h, we did not detect differences in Rab18 knockout and wild-type cells (Figure 5, A and B).

We also analyzed the amounts of free fatty acids released into the culture medium (using radioactive oleate as tracer material) and, consistent with the microscopy studies, detected no major differences between Rab18 and wild-type cells with respect to TG consumption or fatty acid release (Figure 5, C–E).

In the current study, we found little effects of deleting Rab18 on LD biogenesis or turnover in a mammary carcinoma cell line. The most significant phenotype we found was a modest reduction in LD size and numbers with oleate induction of LDs. We also did not find effects of Rab18 deletion on the targeting of several key LD proteins, although we cannot exclude that Rab18 activation at LDs is involved in recruiting other proteins. Considering these data, we conclude that Rab18 is not a necessary component of the basic cell machinery required for LD formation, expansion, or consumption. In comparison, other key components of this machinery, such as seipin, FIT2, or perilipins for LD biogenesis (Bulankina *et al.*, 2009; Gross *et al.*, 2011; Wilfling *et al.*, 2014a; Choudhary *et al.*, 2015; Wang *et al.*, 2016), or Arf1/COPI proteins for ER-LD targeting (Wilfling *et al.*, 2014b), have prominent effects on cells and tissues that store neutral lipids. Homozygous Rab18 knockout mice show an eye and neuronal phenotypes, and embryonic fibroblasts derived from this line have a mildly affected LD morphology, but neutral lipid storage in liver or adipose tissue is not affected (Carpanini *et al.*, 2014), further arguing against a strong requirement for Rab18 in fundamental LD processes.

In contrast to our findings in SUM159 cells, defects in LD formation were found when Rab18 was knocked out in murine adipocytes, suggesting that Rab18 is an important component of LD growth and maturation in this cell type (Xu *et al.*, 2018). However, consistent with our findings, deficiency of Rab18 in several other mammalian cell lines (AML12, HeLa, Cos7, and 293T) did not show an effect on LDs (Xu *et al.*, 2018).

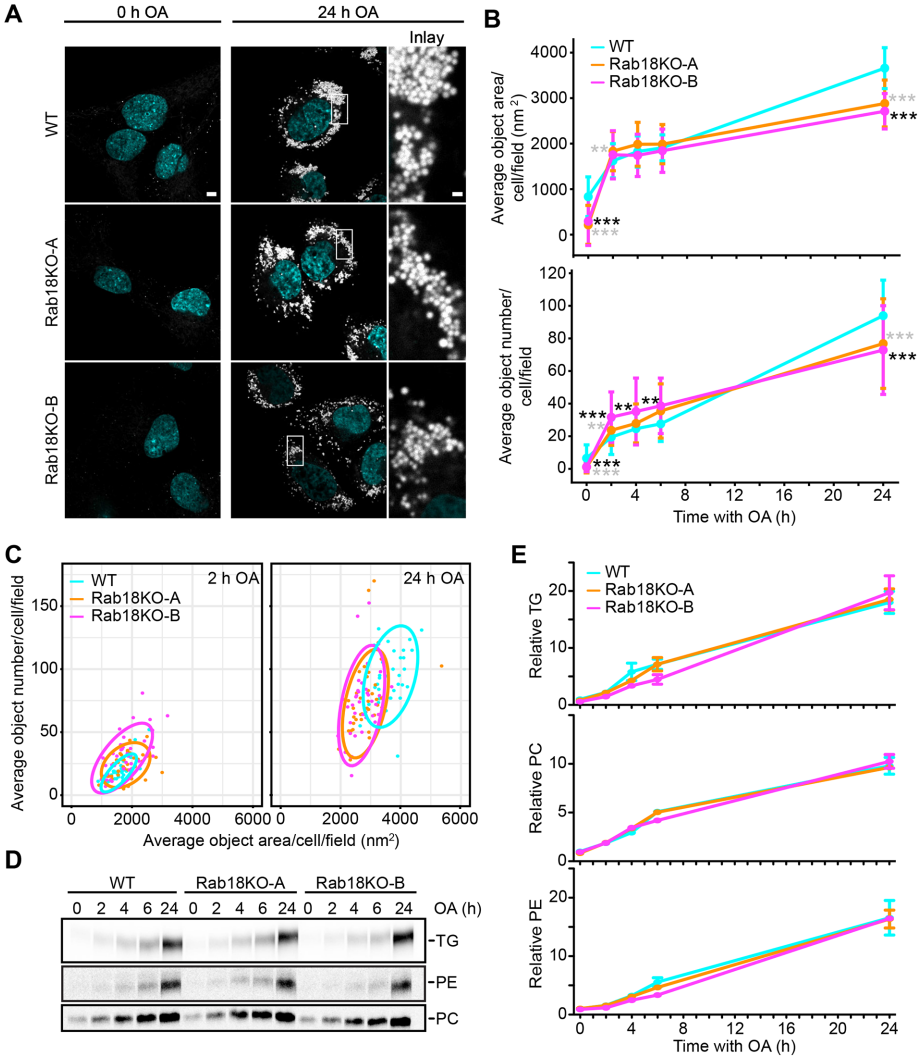

FIGURE 3: LD biogenesis is not affected in Rab18 KO cells. (A) LD morphology is similar in Rab18KO clones and WT cells with oleic acid incubation. Representative images of WT and Rab18 KO cells prestarved for 5 h before addition of oleic acid and after 24 h of oleic acid incubation. Scale bar 5 μm and for inlay 1 μm. (B) Rab18 KO average BODIPY object area and number are slightly smaller than WT after 24 h oleic acid incubation. WT and Rab18 KO cells were incubated with oleic acid for indicated time points, fixed, and imaged by high-throughput microscopy. Average BODIPY object area and number per cell per field (>five cells per field to obtain representative measurements) were quantified per condition. $n > 27$ fields/point. WT vs. Rab18KO-A* in gray; WT vs. Rab18KO-B* in black. (C) Rab18KO and WT average object area vs. number 90% confidence intervals overlap at 2 and 24 h oleic acid incubation. Average object number plotted against average object area per cell per field with 2 and 24 h oleic acid. Ellipses represent 90% confidence intervals. (D, E) Rab18KO clones have similar synthesis of TG, PE, and PC as WT cells with oleic acid incubation. Incorporation of [^{14}C] oleate into triglycerides (TGs), phophatidylethanolamine (PE), and phosphatidycholine (PC) were measure over time. Lipids were extracted from cells and separated by TLC. Representative autoradiographs of three replicates per genotype are shown (D). (E) Quantified TG, PC, and PE levels are similar between Rab18KO clones and WT cells over time. TLC plates were developed and incorporation of [^{14}C] oleate into TGs, PE, and PC was quantified using Fiji. Data presented are normalized CPM to mg/ml protein and relative to WT at $t = 0$ h. $n = 3$.

It is unclear why Rab18 depletion might affect LD formation and maturation in murine adipocytes, but not other cell types, and why it has no dramatic effect on murine adipose tissue. One possibility is that Rab18, while not a component of the basic LD formation machinery in cells, is involved in specific processes of LD growth in specialized cells such as adipocytes, which generate much larger, unilocular LDs (tens of microns diameter) than most cell types (0.5- to 2-μ diameter) using specific machinery, such as CIDE-C/Fsp27 (Nordström *et al.*, 2005; Puri *et al.*, 2007). Thus, Rab18 may be similarly involved in adipocyte-specific processes. An alternative explanation may be that Rab18 has functional redundancy with other Rab proteins in some cells (SUM159, AML12, HeLa, Cos7, and 293T) but not in murine adipocytes. Further studies are needed to clarify the physiological function of Rab18 and to determine the specific downstream molecular consequences of Rab18 recruitment to LD surfaces.

MATERIALS AND METHODS

Antibodies

We used rabbit polyclonal antibodies against Rab18 (Proteintech; 11304-1-AP), ATGL (CST; 2138S), Calnexin (Enzo: ADI-SPA-860), reticulon 4 (Santa Cruz; Nogo N18 SC11027), and glyceraldehyde 3-phosphate dehydrogenase (GAPDH) (Santa Cruz Biotechnology; sc-25778). Tip47 antibody from guinea pig was from Fitzgerald (20RTP001). Mouse (monoclonal) anti–α tubulin was from Sigma (T5168). We used HRP-conjugated secondary antibodies against mouse (Santa Cruz Biotechnology; sc-2004), rabbit (Santa Cruz Biotechnology; sc-516102), and guinea pig (Santa Cruz Biotechnology; sc-2438) for immunoblotting and anti-rabbit Alexa Fluor 488 (Abcam; ab150077) for immunofluorescence.

Plasmids

Human expression vectors were generated by cloning Rab18, Rab18(S22N), Rab18(Q67L), into pEGFP-C1 vector (Clontech) using *Bam*HI and *Sal*I and PLIN3 into pEGFP-C1 vector with pTK promoter using *Kpn*I and *Bam*HI. C-terminal mCherry-tagged ATGL(S47A) was expressed from pcDNA3.1 (Thermo Fisher), C-terminl GFP-tagged human GPAT4 from pcDNA-DEST47 vector (Thermo Fisher), C-terminal GFP-tagged KDEL from oxGFP vector (Addgene #68069), and mCherry-ER3 (Addgene #55041).

Cell culture and transfection

SUM159 cells (RRID:CVCL_5423) were obtained from the laboratory of Tomas Kirchausen (Harvard Medical School) and were maintained in DMEM/F-12 GlutaMAX (Life Technologies) with 5 μg/ml insulin (Cell Applications), 1 μg/ml hydrocortisone (Sigma), 5% FBS (Life Technologies 10082147; Thermo Fisher), 50 μg/ml streptomycin, and 50 U/ml penicillin. Where noted, cells were incubated with media containing 500 μM oleic acid complexed with 0.5% essentially fatty acid free bovine serum albumin (BSA) (Sigma Aldrich). Transfection of plasmids into SUM159 cells was performed with FuGENE HD transfection reagent (Promega) 18–24 h before imaging.

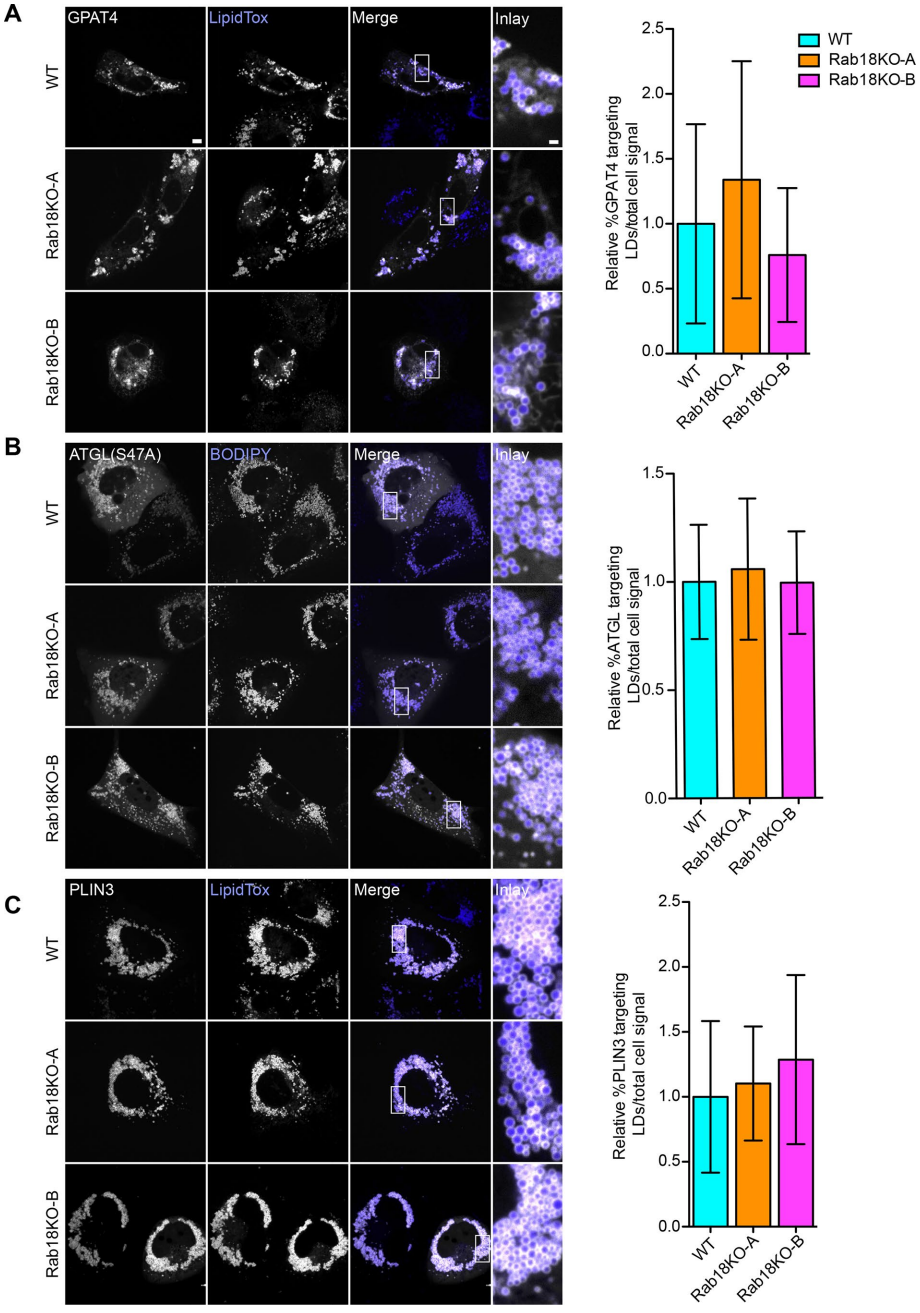

FIGURE 4: Protein targeting to LDs is similar in Rab18KO and WT. (A–C) Representative confocal images of WT, Rab18KO-A, and Rab18KO-B cells transfected with GPAT4-GFP (A), catalytically inactive mCherry-ATGL(S47A) (B), and GFP-PLIN3 (C) were incubated with oleic acid for 24 h. Targeting to LDs stained with LipidTox (A, C) or BODIPY (B) compared with total cell signal quantified in (A) $n \geq 39$ cells, (B) $n \geq 36$ cells, and (C) $n \geq 43$ cells. Scale bar 5 µm and for inlay 1 µm.

Generating Rab18 knockouts in SUM159 cells

Three independent targeting sequences to direct Cas9 to exons 4, 5, and 7 of the Rab18 locus were used simultaneously as guide RNA (gRNA) in the Cas9 and gRNA expression plasmid px459 (Addgene) (primer sequences: exon 4, CACCGGAAATAGTCCAAT CCTGAAG, AAACCTTCAGGATTGGACTATTTCC; exon 5, CACCGCTGTGCAC CTCTATAATAGC, AAACGCTATTATAGAGGTGCACAGC; exon 7, CACCGCG TGAAGTCGATAGAAATGA, AAACTCATTTCTAT CGACTTCACGC). Either 600 µg of each gRNA px459 plasmid or 1 µg of empty px459 plasmid was transfected into 80,000 cells. Transfected cells were isolated by treatment with puromycin for 4 d, followed by single-cell sorting using flow-cell cytometry (FACSAria II; BD Biosciences) as described (Ran *et al.*, 2013). Knockout clones were verified by Western blot analysis of cell lysates using Rab18 antibodies and sequencing of PCR-amplified gRNA target regions subcloned into pCR Blunt II TOPO vector (Thermo Fisher Scientific). Positive clones were verified by quantitative PCR (qPCR) (sense primer: CCATGTTATTTATAGAGGCAAGTG, and anti-sense primer: CAAGTTCTTCAAAGGCACATT) using power SYBR green (Life Technologies). For all experiments with Rab18 knockout cells, wild-type cells transfected with an empty px459 plasmid were used as control wild-type cells.

Imaging and image analysis

Live cell imaging was performed on a Nikon Eclipse Ti inverted microscope equipped with a CSU-X1 spinning disk confocal head (Yokogawa); 405-, 488-, 561-, or 639-nm laser lines; 100× ApoTIRF 1.4 NA objective (Nikon, Melville, NY); and iXon Ultra 897 electron-multiplying charge-coupled device (EMCCD) or Zyla 4.2 Plus scientific complementary metal-oxide semiconductor (sCMOS) cameras (Andor, Belfast, UK). Cells were annually tested for mycoplasma contamination by Universal Mycoplasma Detection Kit (American Type Culture Collection). For quantification of ER morphology, 3-µm Z stacks with 0.25-µm steps were acquired.

Imaging experiments of SUM159 cells were carried out in Life Technologies Fluorobrite DMEM (Life Technologies) supplemented with SUM159 maintenance media components. LDs were stained with 0.5 µg/ml BODIPY 493/503 (Life Technologies) or HCS LipidTOX Deep Red Neutral Lipid Stain (Thermo Fisher Scientific) 20 min prior to imaging. Nuclei were stained with 1 µg/ml Hoechst 33342 (Thermo Fisher).

For immunofluorescence experiments cells were fixed in 4% formaldehyde (Polysciences) for 20 min at room temperature (RT), followed by permeabilization and staining as described previously (Wilfling *et al.*, 2013). Slides were mounted with ProLong Gold Antifade mounting medium with 4′,6-diamidino-2-phenylindole (DAPI) (Thermo Fisher Scientific) and stored at 4°C.

High-throughput imaging was performed on an IN CELL Analyzer 6000 microscope (GE Healthcare Life Sciences) using a 60 × 0.95 NA objective. Cells were fixed in 4% formaldehyde (Polysciences) at RT for 20 min, washed three times, with phosphate-buffered saline (PBS), and stained for LDs and nuclei as described above. Twenty-four to 64 images were acquired per well.

SIM of living cells was performed on an OMX V4 Blaze (GE Healthcare Life Sciences) equipped with three PCO.edge sCMOS

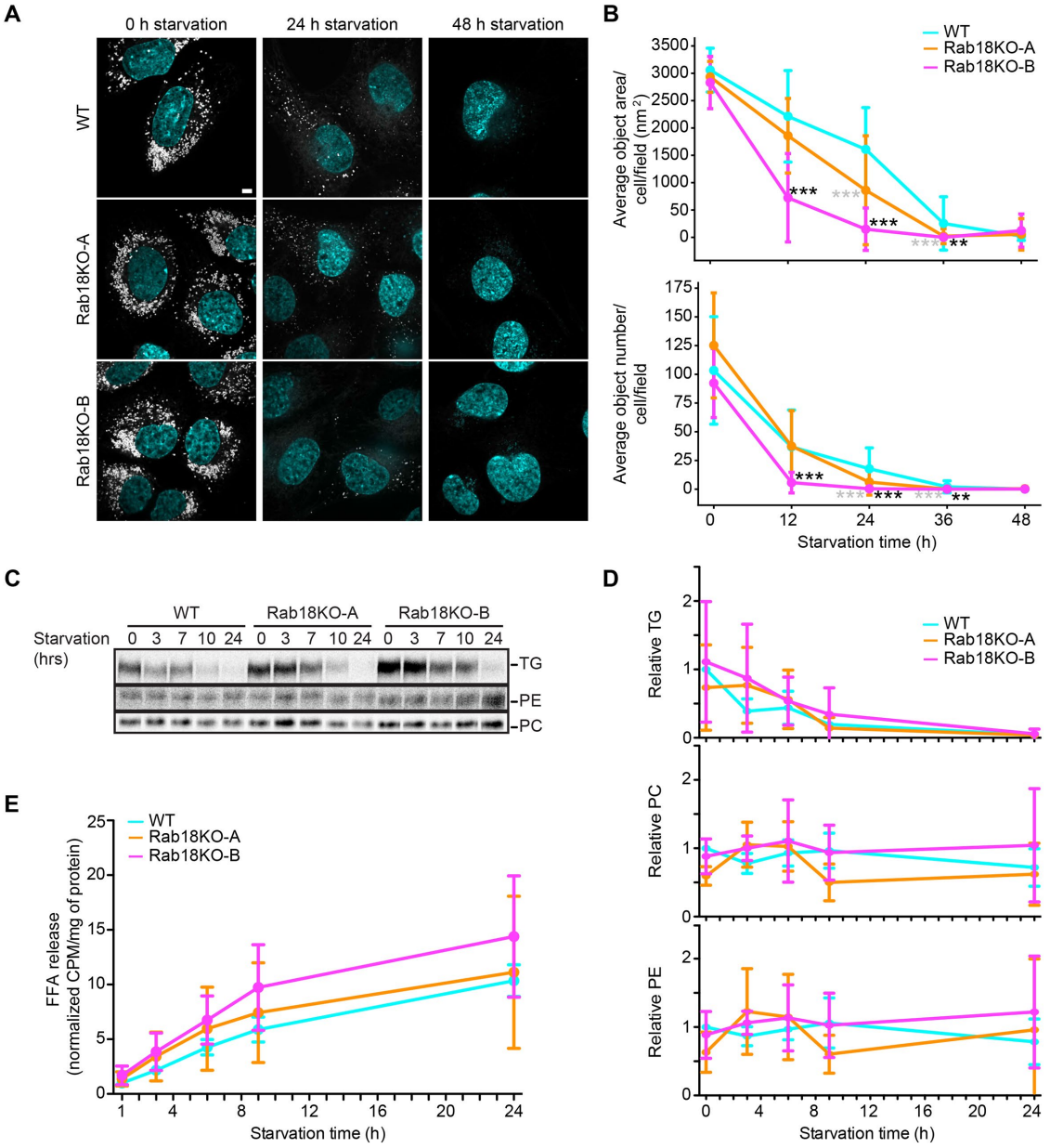

FIGURE 5: Rab18 deletion does not affect TG turnover. (A) LDs are degraded similarly in Rab18KO clones and WT cells with starvation. Representative images of WT, Rab18KO-A, and Rab18KO-B cells after 12 h OA loading ($t = 0$) and 24 or 48 h of starvation. LDs stained with BODIPY 493/503 and nuclei with Hoechst. Scale bar 5 μm and inlay 1 μm. (B) Rab18KO average BODIPY object area and number are similar to WT after 48 h starvation. WT and Rab18KO cells were incubated with oleic acid for indicated time points as in A. Cells were fixed and imaged by high-throughput microscopy. Average BODIPY object area and number per cell per field (>5 cells per field) was quantified per condition. $n > 7$ fields. WT vs. Rab18KO-A * in gray; WT vs. Rab18KO-B * in black. (C) Rab18KO clones have similar synthesis of TG and PE and less PC than WT cells with starvation. WT and Rab18KO cells were incubated with [^{14}C] oleic acid for 18 h, followed by starvation for increasing time. Total lipids were extracted at each time point and separated by TLC to detect radiolabeled TG, PE, and PC levels. Representative autoradiographs of three replicates per genotype. (D) Quantified TG and PE levels are similar, and PC levels are less between Rab18KO clones and WT cells over time with starvation. TG, PC, and PE signals were quantified from TLC plates using Fiji. Data presented are normalized CPM to mg/ml protein and relative to WT at $t = 0$ h. $n = 3$ biological replicates. (E) Rab18KO clones have decreased free fatty acid release over time with starvation. The [^{14}C]-labeled free fatty acid release measured over time with starvation after WT; Rab18KO-A, and Rab18KO-B cells were incubated with [^{14}C] oleic acid for 18 h. $n = 3$ biological replicates.

cameras, 488- and 568-nm laser lines, and a 60 × 1.42 Plan Apochromat objective (Olympus). Usually 2.5-μm stacks with 0.125-μm step size with 15 raw images (three rotations with five phases each) per z-section were acquired. Spherical aberration was minimized by immersion oil matching (Hiraoka *et al.*, 1990). Superresolution images were reconstructed from raw data sets with channel specific, measured optical transfer function and Wiener filter constant of 0.001 using a CUDA-accelerated three-dimensional SIM

reconstruction code based on Gustafsson *et al.* (2008). TetraSpeck beads (Thermo Fisher) or a nano-grid control slide (GE) were used to measure axial and lateral chromatic misregistration. Experimental data sets were registered using the imwarp function in MATLAB (MathWorks).

For image analysis, LD area and number from high-throughput microscopy images were quantified using CellProfiler software (Carpenter *et al.*, 2006). Two workflows were developed for analysis of images from oleic acid (OA) loading conditions and from starvation conditions. Rab18 localization in SIM images was quantified by segmenting mCherry-ER3 and GFP-Rab18 signals of sum projections from 0.375-µm stacks using Huang's threshold. Total Rab18 integrated density was measured in the combined Rab18 and ER area, while LD integrated density was calculated in total area without the ER area.

Protein targeting was quantified using FIJI software (Schindelin *et al.*, 2012). To identify the region of LDs, a threshold was applied to the BODIPY or LipidTox channels as developed by Prévost *et al.* (2018). The mean intensity of mCherry or GFP protein signal within the LD region was measured and divided by the mean intensity of the total signal in the cell.

Metabolic labeling and analysis of lipids

Incorporation of TG during fatty acid loading was measured by addition of 500 µM [^{14}C] oleic acid (25 µCi/µmol), followed by lipid and protein extraction in hexane/isopropanol (3:2) or radioimmunoprecipitation assay (RIPA) buffer, respectively. Lipid loading to thin-layer chromatography (TLC) plates (Merck) was normalized to total protein. Phospholipids were separated in $CHCl_3/CH_3OH/H_2O$ (65:35:4) and neutral lipids in hexane/diethyl ether/acetic acid (80:20:1). TLC plates were exposed to imaging screens and scanned in a Typhoon FLA 7000 (GE Healthcare) to visualize radioactive compounds. For starvation experiments, cells were incubated with 500 µM [^{14}C] oleic acid (25 µCi/µmol) for 16 h, followed by three washes with PBS and addition of starvation medium (DMEM low glucose, 10 mM HEPES, pH 7.0, 1% penicillin and streptomycin, 1% essentially fatty acid-free BSA). At each time point, lipids and proteins were extracted as described above. To measure free fatty acid release, 10% of medium was collected, and radioactivity was measured in a Hidex 300SL liquid scintillation counter (Hidex). Radioactivity was measured and counts per minute (CPM) measurements were normalized to mg/ml protein.

Subcellular fractionation

Cells were harvested, washed once with ice-cold PBS followed by a wash in homogenization buffer (20 mM Tris-HCl, pH 7.4, 250 mM sucrose, 1 mM EDTA, pH 8, Roche complete protease inhibitor tablet), and followed by resuspension in 1 ml of homogenization buffer (HB) and lysis through a 23G needle 30 times. NaCl was added to final concentration of 100 mM, and lysates were cleared for 10 min, 1000 × *g* and 8000 × *g* to remove unlysed cells, nuclei, and mitochondria. Cleared lysate was subjected to ultracentrifugation for 1 h at 100,000 × *g* at 4°C. The pellet was resuspended in homogenization buffer, followed by SDS–PAGE and Western blot analysis. To purify LDs, the 100,000 × *g* supernatant was mixed 1:1 with 50% OptiPrep in HB and layered with 500 µl 16% OptiPrep, 1.5 ml 8% OptiPrep, 500 µl 2% OptiPrep, and 500 µl HB. Gradients were subjected to ultracentrifugation in a swinging bucket rotor (TLS55, Beckman-Coulter) for 16 h at 150,000 × *g* at 4°C. LDs were collected from the top layer. Protein was precipitated from this layer, and the remaining layers collectively to analyze the cytosol (Wessel and Flügge, 1984). Protein concentration was determined by Bradford or absorption at 280 nm (nanodrop; Thermo Fisher Scientific).

Mass spectrometry analyses of total cell lysates and LDs

Precipitated proteins from total cell lysates and purified LD fractions were resolubilized in 100 mM NaOH aided by sonication at 4°C, and the solution was brought to pH 7.5 with 200 mM HEPES (4-(2-hydroxyethyl)-1-piperazineethanesulfonic acid). Proteins were reduced using 5 mM dithiothreitol (Sigma-Aldrich) at 37°C for 1 h, followed by alkylation of cysteine residues using 15 mM iodoacetamide (Sigma-Aldrich) in the dark at RT for 1 h. Excessive iodoacetamide was quenched using 10 mM dithiotheritol. Protein mixtures were diluted in 1:6 ratio (vol/vol) using ultrapure water prior to digestion using sequencing grade trypsin (Promega) at 37°C for 16 h. Digested peptides were subsequently desalted using self-packed C18 STAGE tips (3M Empore) for liquid chromatography–mass spectrometry (LC-MS)/MS analysis (Rappsilber *et al.*, 2003). Desalted peptides were resuspended in 0.1% (vol/vol) formic acid and loaded onto a high-performance liquid chromatography tandem mass spectrometry (HPLC-MS/MS) system for analysis on an Orbitrap Q-Exactive HF (Thermo Fisher Scientific) mass spectrometer coupled to an Easy nanoLC 1000 (Thermo Fisher Scientific) with a flow rate of 300 nl/min. The stationary phase buffer was 0.5% formic acid, and mobile phase buffer was 0.5% (vol/vol) formic acid in acetonitrile. Chromatography for peptide separation was performed using increasing organic proportion of acetonitrile (5–40% [vol/vol]) over a 265-min gradient) on a self-packed analytical column using a PicoTip emitter (New Objective, Woburn, MA) using Reprosil Gold 120 C-18, 1.9-µm particle size resin (Dr. Maisch, Ammerbuch-Entringen, Germany). The mass spectrometry analyzer operated in data-dependent acquisition mode with a top 10 method at a mass range of 300–2000 Da.

Mass spectrometry data were processed by MaxQuant software version 1.5.2.8 (Cox and Mann, 2008) with the following settings: oxidized methionine residues and protein N-terminal acetylation as variable modification, cysteine carbamidomethylation as fixed modification, first search peptide tolerance 20 ppm, and main search peptide tolerance 4.5 ppm. Protease specificity was set to trypsin with up to two missed cleavages were allowed. Only peptides longer than five amino acids were analyzed, and the minimal ratio count to quantify a protein is 2 (proteome only). The false discovery rate was set to 1% for peptide and protein identifications. Database searches were performed using the Andromeda search engine integrated into the MaxQuant environment (Cox *et al.*, 2011) against the UniProt-human database containing 71,579 entries (October 2017). "Matching between runs" algorithm with a time window of 0.7 min was employed to transfer identifications between samples processed using the same nanospray conditions. Protein tables were filtered to eliminate identifications from the reverse database and also common contaminants. Mass spectrometry source files generated were deposited to the ProteomeXchange Consortium via the PRIDE partner repository (Vizcaíno *et al.*, 2016) with the data set identifier PXD009683.

Statistical analysis

Data are presented as mean ± SD. Statistical significance of qPCR data was analyzed by unpaired two-tailed Student's *t* test. For high-throughput imaging data that were not normally distributed, the nonparametric Wilcoxon rank-sum test for single comparisons was used. The following analyses for normally distributed data were performed using GraphPad Prism 5.0: for free fatty acid release from

the same samples over time, statistical significance was evaluated by repeated measures two-way analysis of variance (ANOVA); for quantification of protein targeting, one-way ANOVA followed by the Tukey post-hoc test. For all other data involving multiple comparisons, statistical significance was evaluated by two-way ANOVA followed by the Bonferroni post-hoc test. For all analyses, values of $p < 0.01$ were considered statistically significant, $^{**}p < 0.01$; $^{***}p < 0.001$. All experiments were repeated at least two independent times.

ACKNOWLEDGMENTS

We thank Hugo B. Brandão for help with data analysis; Chandramohan Chitraju for help with experiments; members of the Farese and Walther laboratory for discussions; the Sabri Ülker imaging center; the Image and Data Analysis Core at Harvard Medical School (HMS); Stephanie Mohr from the *Drosophila* RNAi Screening Center at HMS (National Institutes of Health National Institute of General Medical Sciences R01 GM067761); Lin Shao (Yale University) for CUDA-accelerated 3D-SIM reconstruction code, Talley Lambert and Jennifer Waters in the Cell Biology Microscopy Facility at HMS, and Gary Howard for editorial assistance. This work was supported by the National Institutes of Health National Institute of General Medical Sciences through R01GM124348-01 (to R.V.F.) and 1R01GM097194 (to T.C.W.). T.C.W. is an investigator of the Howard Hughes Medical Institute. C.K.J. was supported by the National Science Foundation Graduate Research Fellowship under Grant No. DGE1144152 and the Department of Defense through the National Defense Science & Engineering Graduate Fellowship (NDSEG). H.A. was supported by a German Research Foundation (DFG) research fellowship (AR1164/1-1) and A.W.F. by a travel grant from the DFG graduate school GRK 1459 and a PhD fellowship from the German Academic Scholarship Foundation.

REFERENCES

Barr FA (2013). Rab GTPases and membrane identity: causal or inconsequential? J Cell Biol 202, 191–199.

Bulankina AV, Deggerich A, Wenzel D, Mutenda K, Wittmann JG, Rudolph MG, Burger KNJ, Höning S (2009). TIP47 functions in the biogenesis of lipid droplets. J Cell Biol 185, 641–655.

Bussell R (2005). Helix periodicity, topology, and dynamics of membrane-associated-Synuclein. Protein Sci 14, 862–872.

Carpanini SM, McKie L, Thomson D, Wright AK, Gordon SL, Roche SL, Handley MT, Morrison H, Brownstein D, Wishart TM, *et al.* (2014). A novel mouse model of Warburg Micro syndrome reveals roles for RAB18 in eye development and organisation of the neuronal cytoskeleton. Dis Model Mech 7, 711–722.

Carpenter AE, Jones TR, Lamprecht MR, Clarke C, Kang IH, Friman O, Guertin DA, Chang JH, Lindquist RA, Moffat J, Golland P, Sabatini DM (2006). CellProfiler: image analysis software for identifying and quantifying cell phenotypes. Genome Biol 7, R100.

Choudhary V, Ojha N, Golden A, Prinz WA (2015). A conserved family of proteins facilitates nascent lipid droplet budding from the ER. J Cell Biol 211, 261–271.

Čopič A, Antoine-Bally S, Giménez-Andrés M, La Torre Garay C, Antonny B, Manni MM, Pagnotta S, Guihot J, Jackson CL (2018). A giant amphipathic helix from a perilipin that is adapted for coating lipid droplets. Nat Commun 9, 1–16.

Cox J, Mann M (2008). MaxQuant enables high peptide identification rates, individualized p.p.b.-range mass accuracies and proteome-wide protein quantification. Nat Biotechnol 26, 1367–1372.

Cox J, Neuhauser N, Michalski A, Scheltema RA, Olsen JV, Mann M (2011). Andromeda: a peptide search engine integrated into the MaxQuant environment. J Proteome Res 10, 1794–1805.

Flanagan L, Van Weelden K, Ammerman C, Ethier SP, Welsh JE (1999). SUM-159PT cells: a novel estrogen independent human breast cancer model system. Breast Cancer Res Treat 58, 193–204.

Gerondopoulos A, Bastos RN, Yoshimura SI, Anderson R, Carpanini S, Aligianis I, Handley MT, Barr FA (2014). Rab18 and a Rab18 GEF complex are required for normal ER structure. J Cell Biol 205, 707–720.

Gillingham AK, Sinka R, Torres IL, Lilley KS, Munro S (2014). Toward a comprehensive map of the effectors of rab GTPases. Dev Cell 31, 358–373.

Gluchowski NL, Becuwe M, Walther TC, Farese RV (2017). Lipid droplets and liver disease: from basic biology to clinical implications. Nat Rev Gastroenterol Hepatol 14, 343–355.

Gross DA, Silver DL (2014). Cytosolic lipid droplets: From mechanisms of fat storage to disease. Crit Rev Biochem Mol Biol 49, 304–326.

Gross DA, Zhan C, Silver DL (2011). Direct binding of triglyceride to fat storage-inducing transmembrane proteins 1 and 2 is important for lipid droplet formation. Proc Natl Acad Sci USA 108, 19581–19586.

Gustafsson MGL, Shao L, Carlton PM, Wang CJR, Golubovskaya IN, Cande WZ, Agard DA, Sedat JW (2008). Three-dimensional resolution doubling in wide-field fluorescence microscopy by structured illumination. Biophys J 94, 4957–4970.

Hiraoka Y, Sedat JW, Agard DA (1990). Determination of three-dimensional imaging properties of a light microscope system. Partial confocal behavior in epifluorescence microscopy. Biophys J 57, 325–333.

Hönscher C, Mari M, Auffarth K, Bohnert M, Griffith J, Geerts W, van der Laan M, Cabrera M, Reggiori F, Ungermann C (2014). Cellular metabolism regulates contact sites between vacuoles and mitochondria. Dev Cell 30, 86–94.

Hutagalung AH, Novick PJ (2011). Role of Rab GTPases in membrane traffic and cell physiology. Physiol Rev 91, 119–149.

Kassan A, Herms A, Fernández-Vidal A, Bosch M, Schieber NL, Reddy BJN, Fajardo A, Gelabert-Baldrich M, Tebar F, Enrich C, *et al.* (2013). Acyl-CoA synthetase 3 promotes lipid droplet biogenesis in ER microdomains. J Cell Biol 203, 985–1001.

Kory N, Farese RV, Walther TC (2016). Targeting fat: mechanisms of protein localization to lipid droplets. Trends Cell Biol 26, 535–546.

Li C, Luo X, Zhao S, Siu GK, Liang Y, Chan HC, Satoh A, Yu SS (2016). COPI–TRAPPII activates Rab18 and regulates its lipid droplet association. EMBO J 36, 441–457.

Martin S, Driessen K, Nixon SJ, Zerial M, Parton RG (2005). Regulated localization of Rab18 to lipid droplets: Effects of lipolytic stimulation and inhibition of lipid droplet catabolism. J Biol Chem 280, 42325–42335.

Nordström EA, Rydén M, Backlund EC, Dahlman I, Kaaman M, Blomqvist L, Cannon B, Nedergaard J, Arner P (2005). A human-specific role of cell death-inducing DFFA (DNA fragmentation factor-α)-like effector A (CIDEA) in adipocyte lipolysis and obesity. Diabetes 54, 1726–1734.

Ozeki S, Cheng J, Tauchi-Sato K, Hatano N, Taniguchi H, Fujimoto T (2005). Rab18 localizes to lipid droplets and induces their close apposition to the endoplasmic reticulum-derived membrane. J Cell Sci 118, 2601–2611.

Pfeffer SR (2001). Rab GTPases: Specifying and deciphering organelle identity and function. Trends Cell Biol 11, 487–491.

Pol A, Gross SP, Parton RG (2014). Biogenesis of the multifunctional lipid droplet: Lipids, proteins, and sites. J Cell Biol 204, 635–646.

Prévost C, Sharp ME, Kory N, Lin Q, Voth GA, Farese RV, Walther TC (2018). Mechanism and determinants of amphipathic helix-containing protein targeting to lipid droplets. Dev Cell 44, 73–86.

Pulido MR, Diaz-Ruiz A, Jiménez-Gómez Y, Garcia-Navarro S, Gracia-Navarro F, Tinahones F, López-Miranda J, Frühbeck G, Vázquez-Martínez R, Malagón MM (2011). Rab18 dynamics in adipocytes in relation to lipogenesis, lipolysis and obesity. PLoS One 6, e22931.

Puri V, Konda S, Ranjit S, Aouadi M, Chawla A, Chouinard M, Chakladar A, Czech MP (2007). Fat-specific protein 27, a novel lipid droplet protein that enhances triglyceride storage. J Biol Chem 282, 34213–34218.

Ran FA, Hsu PD, Wright J, Agarwala V, Scott DA, Zhang F (2013). Genome engineering using the CRISPR-Cas9 system. Nat Protoc 8, 2281–2308.

Rappsilber J, Ishihama Y, Mann M (2003). Stop And Go Extraction tips for matrix-assisted laser desorption/ionization, nanoelectrospray, and LC/MS sample pretreatment in proteomics. Anal Chem 75, 663–670.

Rowe ER, Mimmack ML, Barbosa AD, Haider A, Isaac I, Ouberai MM, Thiam AR, Patel S, Saudek V, Siniossoglou S, *et al.* (2016). Conserved amphipathic helices mediate lipid droplet targeting of perilipins 1-3. J Biol Chem 291, 6664–6678.

Schindelin J, Arganda-Carreras I, Frise E, Kaynig V, Longair M, Pietzsch T, Preibisch S, Rueden C, Saalfeld S, Schmid B, *et al.* (2012). Fiji: an open-source platform for biological-image analysis. Nat Methods 9, 676–682.

Schweiger M, Schoiswohl G, Lass A, Radner FPW, Haemmerle G, Malli R, Graier W, Cornaciu I, Oberer M, Salvayre R, *et al.* (2008). The C-terminal

region of human adipose triglyceride lipase affects enzyme activity and lipid droplet binding. J Biol Chem 283, 17211–17220.
Smirnova E, Goldberg EB, Makarova KS, Lin L, Brown WJ, Jackson CL (2006). ATGL has a key role in lipid droplet/adiposome degradation in mammalian cells. EMBO Rep 7, 106–113.
Soldati T, Rancano C, Geissler H, Pfeffer SR (1995). Rab7 and Rab9 are recruited onto late endosomes by biochemically distinguishable processes. J Biol Chem 270, 25541–25548.
Soni KG, Mardones GA, Sougrat R, Smirnova E, Jackson CL, Bonifacino JS (2009). Coatomer-dependent protein delivery to lipid droplets. J Cell Sci 122, 1834–1841.
Stenmark H (2009). Rab GTPases as coordinators of vesicle traffic. Nat Rev Mol Cell Biol 10, 513–525.
Stone SJ, Levin MC, Zhou P, Han J, Walther TC, Farese RV (2009). The endoplasmic reticulum enzyme DGAT2 is found in mitochondria-associated membranes and has a mitochondrial targeting signal that promotes lis association with mitochondria. J Biol Chem 284, 5352–5361.
Tauchi-Sato K, Ozeki S, Houjou T, Taguchi R, Fujimoto T (2002). The surface of lipid droplets is a phospholipid monolayer with a unique fatty acid composition. J Biol Chem 277, 44507–44512.
Vizcaíno JA, Csordas A, Del-Toro N, Dianes JA, Griss J, Lavidas I, Mayer G, Perez-Riverol Y, Reisinger F, Ternent T, *et al*. (2016). 2016 update of the PRIDE database and its related tools. Nucleic Acids Res 44, D447–D456.
Walther TC, Farese RV (2012). Lipid droplets and cellular lipid metabolism. Annu Rev Biochem 81, 687–714.
Wang H, Becuwe M, Housden BE, Chitraju C, Porras AJ, Graham MM, Liu XN, Thiam AR, Savage DB, Agarwal AK, *et al*. (2016). Seipin is required for converting nascent to mature lipid droplets. Elife 5, 133–150.
Wessel D, Flügge UI (1984). A method for the quantitative recovery of protein in dilute solution in the presence of detergents and lipids. Anal Biochem 138, 141–143.
Wilfling F, Haas JT, Walther TC, Jr RVF. (2014a). Lipid droplet biogenesis. Curr Opin Cell Biol 29, 39–45.
Wilfling F, Thiam AR, Olarte MJ, Wang J, Beck R, Gould TJ, Allgeyer ES, Pincet F, Bewersdorf J, Farese RV Jr, Walther TC (2014b). Arf1/COPI machinery acts directly on lipid droplets and enables their connection to the ER for protein targeting. Elife 3, e01607.
Wilfling F, Wang H, Haas JT, Krahmer N, Gould TJ, Uchida A, Cheng JX, Graham M, Christiano R, Fröhlich F, *et al*. (2013). Triacylglycerol synthesis enzymes mediate lipid droplet growth by relocalizing from the ER to lipid droplets. Dev Cell 24, 384–399.
Xu D, Li Y, Wu L, Li Y, Zhao D, Yu J, Huang T, Ferguson C, Parton RG, Yang H, *et al*. (2018). Rab18 promotes lipid droplet (LD) growth by tethering the ER to LDs through SNARE and NRZ interactions. J Cell Biol 217, 975–995.